An Experimental Study on the Flow Characteristics of a Supersonic Turbine Cascade as Pressure Ratio

Jong-Jae Cho*, Soo-In Jeong* and Kui-Soon Kim**
Department of Aerospace Engineering,
Pusan Nation University, Busan, Korea 609-735

Eun-Seok Lee***
Korea Aerospace Research Institute

Abstract

In this paper, a small supersonic wind tunnel was designed and built to study the flow characteristics of a supersonic impulse turbine cascade by experiment. The flow was visualized by means of a single pass Schlieren system. The supersonic cascade with 3-dimensional supersonic nozzle was tested over a wide range of pressure ratio. Highly complicated flow patterns including shocks, nozzle-cascade interaction and shock boundary layer interactions were observed.

Key Word : Supersonic, Cascade, Visualization, Schlieren, Shadowgraph, Shock

Introduction

Conventional turbines operate with subsonic or transonic rotor inlet relative velocities. A recent need for high power turbines for airborne application has renewed the need for a supersonic turbine. The main feature of supersonic turbine is high specific power output with low efficiency. So it is necessary for the power generation with low weight and low inertia for fast start. Propellant feed system often employs supersonic turbine in spite of its low efficiency. Other turbo-pump system which supplies high pressure oil also adopts supersonic turbine. Conventional turbines are fully analyzed with many previous experimental and computational studies resulting in various reliable performance data by Langston[1], Kiock[2], Ainley and Mathieson[3], Dunham and Came[4], etc. But the flow characteristics of supersonic turbine are quite different from those of conventional turbines. The studies about the flow characteristics of supersonic turbine were hardly found except C. D. Colclough[5], B. S. Stratford[6], etc. At the present time, there is little reliable performance data available. In order to design a supersonic turbine with better efficiency, the flow characteristics must be fully investigated to supply sufficient performance data.

In this paper, the experiments have been performed to study the effect of pressure ratio on the flow characteristics of a supersonic turbine. Pressure ratio is an important factor of turbine performance. A small supersonic wind tunnel was designed and built to study the flow characteristics of a supersonic impulse turbine cascade by experiment. The flow was visualized by means of a single pass Schlieren system. The supersonic cascade with 3-dimensional supersonic nozzle was tested over a wide range of pressure ratio.

* Graduate student
E-mail : spacecho@pusan.ac.kr, TEL : 051-510-3290, FAX : 051-513-3760
** Professor
*** Senior researcher

Test Apparatus and Method

Test apparatus

A supersonic wind tunnel was designed and built to study the flow characteristics of a supersonic turbine cascade. The schematic of experimental setup is shown in Fig. 1. The test apparatus consists of four parts - four high pressure nitrogen tanks (pressure and volume of each tank is 1500psi and 42liter), intermediate pressure chamber, on/off solenoid valve and test section. And the test section also consists of four parts - nozzle, nozzle adapter, blades and a pair of test section window. The picture of converging-diverging nozzle used in the experiments and the dimensions of nozzle core are shown in Fig. 2 and Fig. 3, respectively. The nozzle throat diameter is 5.85mm and the nozzle exit diameter is 7.6mm. The nozzle area ratio is 1.687. The nozzle core was manufactured of Stainless Steel. Fig. 4 shows the nozzle and nozzle adapter assembly which was designed for easy replacement of nozzles. The installation angle of the assembled nozzle adapter is 26.14°. The blade profile used in the experiments is shown in Fig. 5 and Fig. 6. The blade chord length is 13.7mm and the pitch is 9.56mm. The angle between nozzle adapter and blade suction surface is 25.34°. The blade was made of Aluminum powder alloy. There were two holes on each blade to fix it to the test section windows by pins as shown in Fig. 7. The test section windows were made of Silica glass to acquire clear Schlieren images.

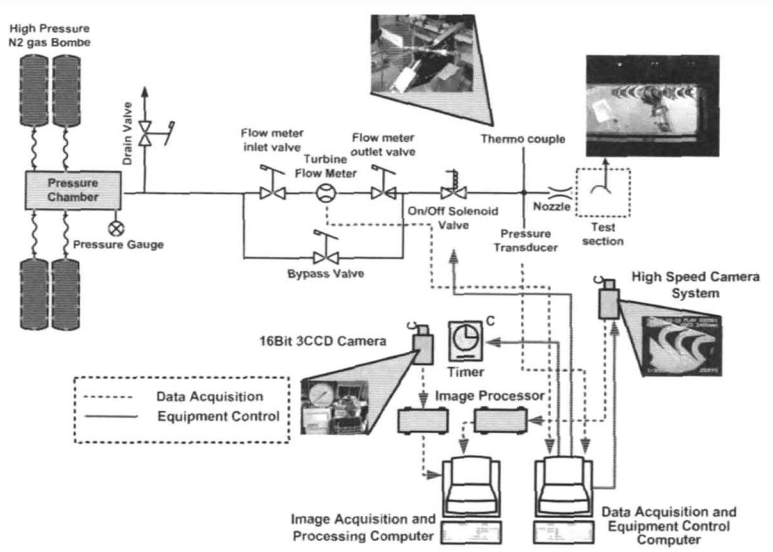

Fig. 1. Schematic of experimental setup

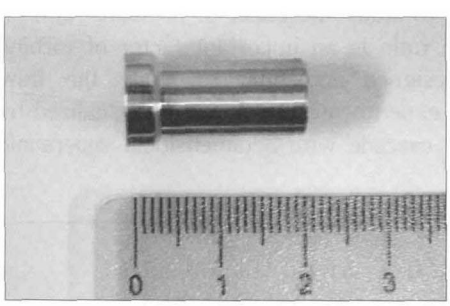

Fig. 2. Nozzle core shape

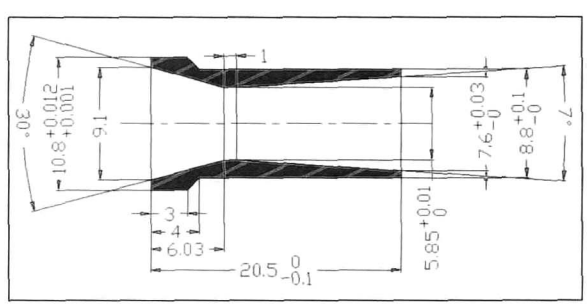

Fig. 3. Nozzle profile

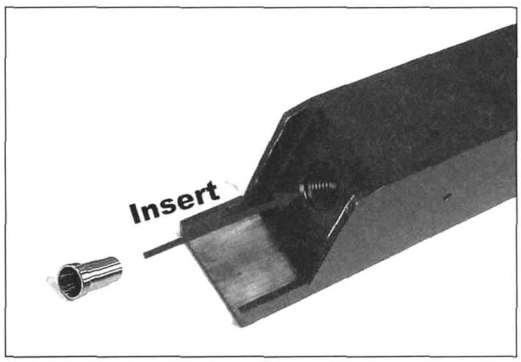

Fig. 4. Nozzle and adapter assemble

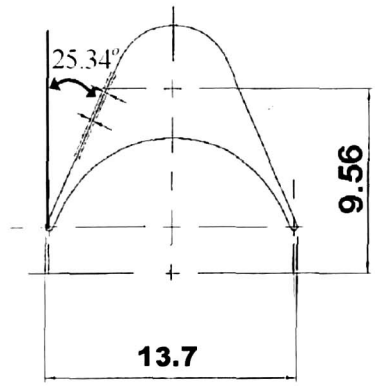

Fig. 5. Blade profile

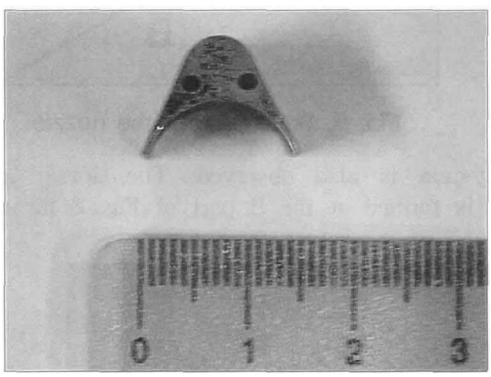

Fig. 6. Blade shape

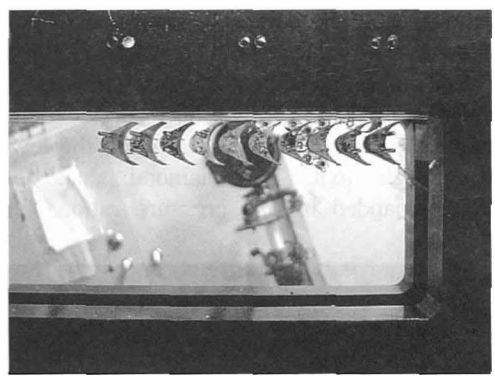

Fig. 7. Test section part

Test procedure and data measurement

All the procedure of the experiments is operated and controlled by a program. After filling the intermediate pressure chamber with nitrogen by opening the valve of nitrogen tanks, the atmospheric pressure was measured for 3 seconds by a pressure transducer (Furness Control Ltd., FC034). And then, the experiments would begin with opening the on/off solenoid valve. At that time, the data such as the mass flow rate, the nozzle inlet static pressure and the total temperature were simultaneously measured by the turbine flow-meter (Flow Technology Inc., LN-5-C-V1-9), the pressure transducer (Kulite, BME-1100-2500SG-A-4) and thermo- couple, respectively. The measured data were transferred directly to the computer through DAQ board. The schematic of equipment for control and measurement is shown in Fig. 1.

Flow visualization and images capture

Shadowgraph and Schlieren system were used for the flow visualization of supersonic turbine cascade in this study. A single Schlieren mirror for Shadowgraph images and a Z-type Schlieren arrangement for Schlieren images were employed. And a continuous 150 watt Tungsten light was also used as light source. Flow images were captured using a 3CCD digital camera (Panasonic, DC330) and a high speed camera system (Kodak, SR Ultra-C). The high speed camera system could capture the images at the maximum speed of 10000 frame/sec. The captured images transformed into digital images and were processed by the image processing computer. All cameras were connected with the computer for data acquisition and equipment control, and they were operated simultaneously when the experiments began. The captured images were compensated by the optical filter of each camera.

Result and Consideration

Nozzle inlet total pressure

The static pressure at the nozzle inlet was measured by a pressure transducer. It can be assumed as total pressure because the Mach number is very small at the measurement position.

Nozzle Flow

The experiments for nozzle flow were executed to find the nozzle flow characteristics with the change of pressure ratio by blowing out the flow to the atmosphere, as shown in Fig. 8. And the experimental results are shown in Fig. 9 ~ Fig. 14.

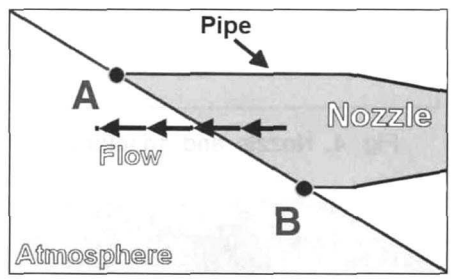

Fig. 8. Schematic of the nozzle

Fig. 9 is the Shadowgraph image for pressure ratio of 4.2. The dark part shown in Fig. 9 is nozzle adapter. The white dot lines represent the position of nozzle core and the axis of nozzle center. Oblique shock is observed at the upper part of the nozzle exit while the flow is expanded around the lower part of the nozzle exit. The diamond shape of shock system is also observed. The nozzle is over-expanded in this pressure ratio. Oblique shock is formed at the B part of Fig. 8 for a

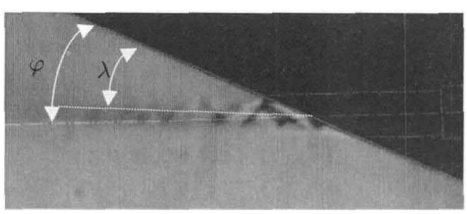

Fig. 9. Nozzle flow (Shadowgraph image) P_{00}:61.68psi, P_1:14.697psi, P_{00}/P_1:4.2

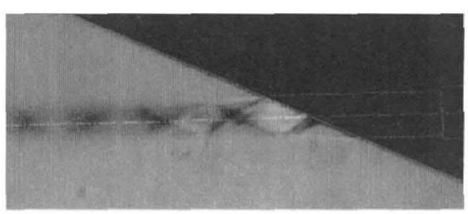

Fig. 10. Nozzle flow (Shadowgraph image) P_{00}:92.52psi, P_1:14.697psi, P_{00}/P_1:6.3

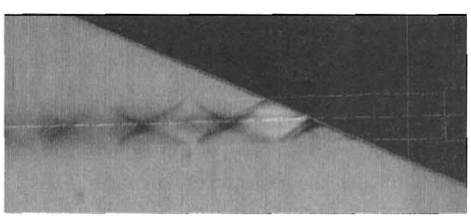

Fig. 11. Nozzle flow (Shadowgraph image) P_{00}:107.94psi, P_1:14.697psi, P_{00}/P_1:7.34

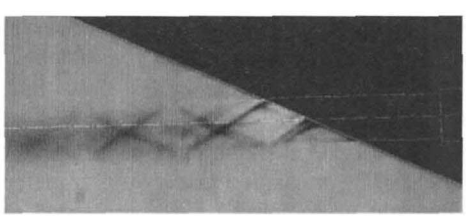

Fig. 12. Nozzle flow (Shadowgraph image) P_{00}:123.36psi, P_1:14.697psi, P_{00}/P_1:8.39

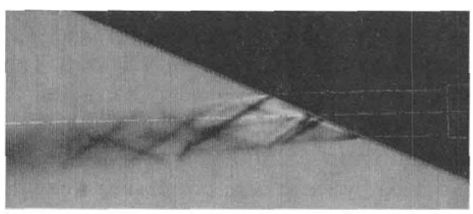

Fig. 13. Nozzle flow (Shadowgraph image) P_{00}:154.2psi, P_1:14.697psi, P_{00}/P_1:10.49

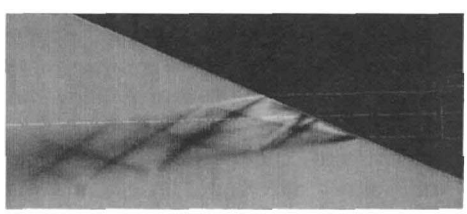

Fig. 14. Nozzle flow (Shadowgraph image) P_{00}:185.04psi, P_1:14.697psi, P_{00}/P_1:12.59

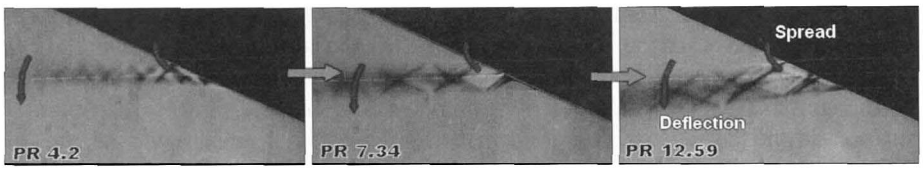

Fig. 15. Nozzle exit flow variation with pressure ratio

recovery to atmospheric pressure. So, nozzle flow is deflected to the upper direction at the point B of Fig. 8 by the oblique shock. And the main flow is deflected to the upper direction. Fig. 10 is the result for pressure ratio of 6.3. The shock system is very close to the result for pressure ratio of 4.2. And the nozzle is also over-expanded. So, nozzle flow is deflected to the upper direction at the point B of Fig. 8 by the oblique shock. But the diamond shape becomes clearer. Nozzle exit flow angle (λ) is still smaller than nozzle installation angle (φ). But the nozzle exit flow angle (λ) is larger than Fig. 9. Fig. 11 is the result for pressure ratio of 7.34. In this case nozzle exit flow angle (λ) is almost same as nozzle installation angle (φ). And the nozzle flow is almost expanded to the exit pressure. Fig. 12 is the result for pressure ratio of 8.39. The nozzle is under-expanded. Expansion wave is occurred at the B part of Fig. 8 for an expansion to exit pressure. So, nozzle flow is deflected to the lower direction at the point B of Fig. 8 by the expansion waves. And the main flow is deflected to the lower direction. The shock system becomes very complex with the shock originated from inside the nozzle . Fig. 13 is the result for pressure ratio of 10.49. The nozzle is also under-expanded. So, nozzle flow is deflected to the lower direction at the point B of Fig. 8 by the expansion waves. And the main flow is deflected to the lower direction. The nozzle exit flow angle (λ) is larger than Fig. 12. And Fig. 14 is the result for pressure ratio of 12.59. The nozzle is also under-expanded. So, nozzle flow is deflected to the lower direction at the point B of Fig. 8 by the expansion wave. And the main flow is deflected to the lower direction. The nozzle exit flow angle (λ) is larger than Fig. 13.

As the pressure ratio increases, the main flow is deflected more to the lower side, and the flow around part A (Fig. 8) is bent more inward with oblique shock while the flow around part B (Fig. 8) is spreaded out more with expansion waves(Fig. 15).

Cascade Experiment

Experiments of the cascade flow were executed to study the flow characteristics within cascade over a wide range of pressure ratio with experimental scheme as shown in Fig. 16. Fig. 18 ~ Fig. 24 show images of the flow visualized by the Shadowgraph system. In case of impulse turbine, P_1 and P_2 are same. So, Experiments were executed under the assumption of P_1 and P_2 of atmospheric pressure.

0(zero) incidence angle was assumed when the blade angle between nozzle adapter and blade suction surface is the same as the nozzle installation angle (φ). The experiments were performed with the blade angle of 25.34° and φ of 26.14°.

Fig. 17 shows the Shadowgraph image of the supersonic cascade flow with negative incidence rotor flow angle. Detached shock is formed at the leading edge of the 2nd blade by the bluntness of the leading edge. And the second shock is observed behind the detached shock. The angle of the detached shock formed at the leading edge of the 1st blade is smaller than that formed at the

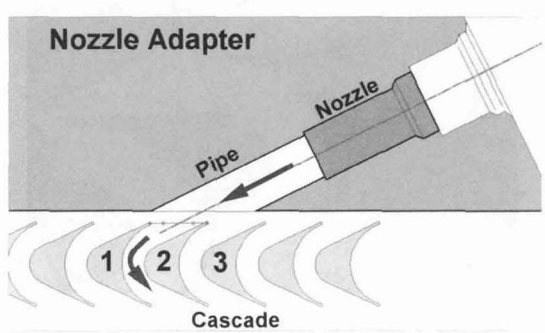

Fig. 16. Schematic of the cascade experiment

leading edge of the 2nd blade. This seemed to be caused by the reason that the angle of the flow at the exit of nozzle decreased by the shocks formed at the leading edge of the 2nd blade. And weak shock is observed at the front of the suction surface of the 2nd blade. This seems to be caused by the gap between the test section windows and blades. Flow is separated form the suction surface at the 35% axial chord downstream from the leading edge of the 2nd blade.

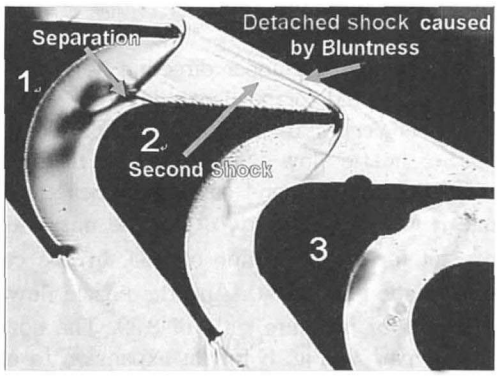

Fig. 17. Cascade flow (Shadowgraph image) P_{00}:205.6psi, P_1:14.696psi, P_{00}/P_1:13.99

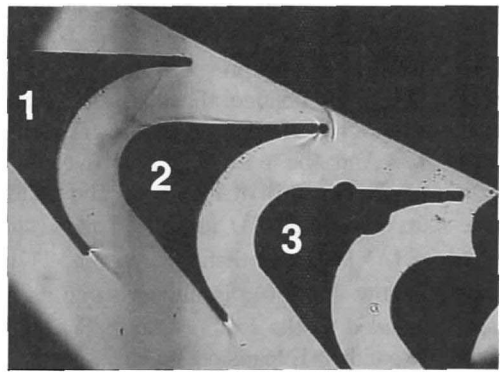

Fig. 18. Cascade flow (Shadowgraph image) P_{00}:61.68psi, P_1:14.696psi, P_{00}/P_1:4.2

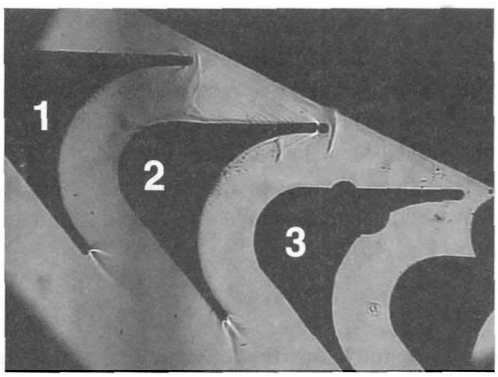

Fig. 19. Cascade flow (Shadowgraph image) P_{00}:77.1psi, P_1:14.696psi, P_{00}/P_1:5.25

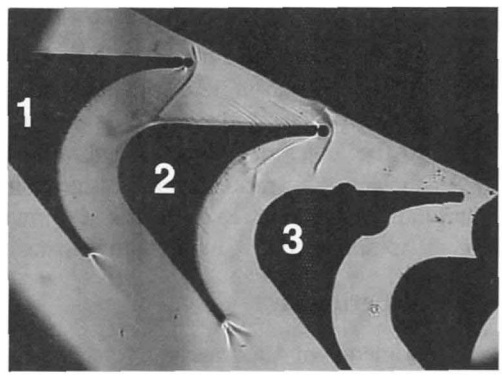

Fig. 20. Cascade flow (Shadowgraph image) P_{00}:92.52psi, P_1:14.696psi, P_{00}/P_1:6.3

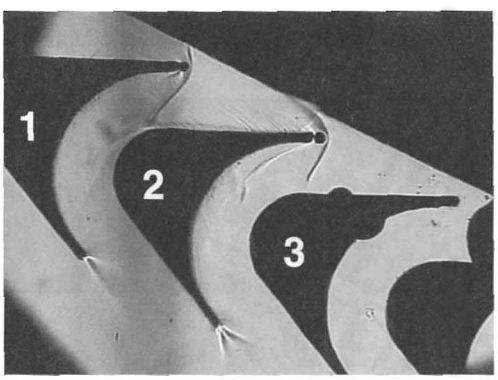

Fig. 21. Cascade flow (Shadowgraph image) P_{00}:107.94psi, P_1:14.696psi, P_{00}/P_1:7.34

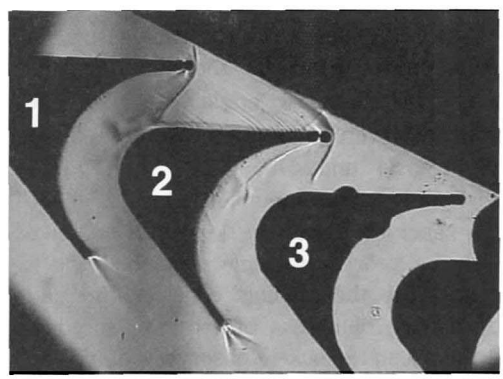

Fig. 22. Cascade flow (Shadowgraph image) P_{00}:123.36psi, P_1:14.696psi, P_{00}/P_1:8.39

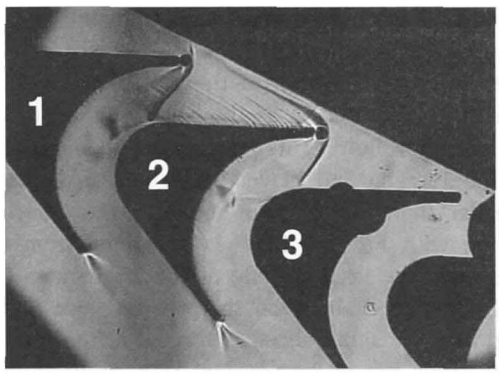

Fig. 23. Cascade flow (Shadowgraph image)
P_{00}:154.02psi, P_1:14.696psi, P_{00}/P_1:10.48

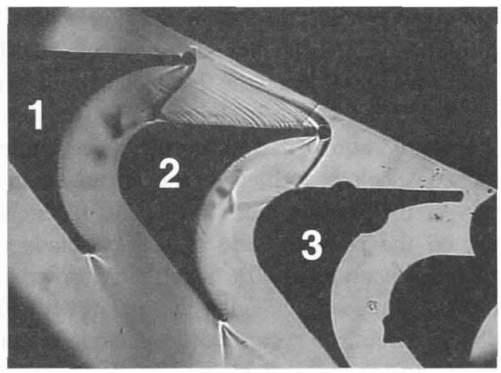

Fig. 24. Cascade flow (Shadowgraph image)
P_{00}:185.04psi, P_1:14.696psi, P_{00}/P_1:12.59

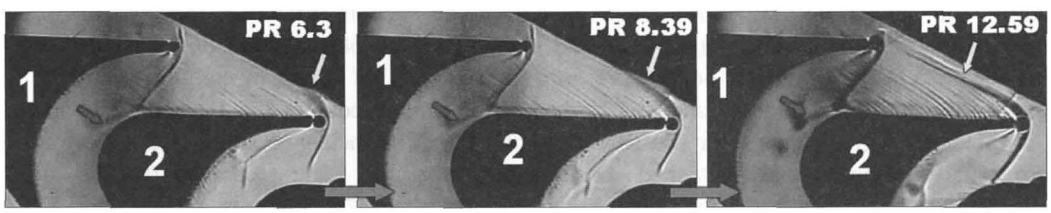

Fig. 25. Cascade flow variation as pressure ratio

Detached shock on the pressure side of the 1st blade meets the separated flow resign on the suction surface of the 2nd blade. Fishtail shocks are observed at the tailing edge of the 1st and 2nd blade. Oblique shocks propagated form the nozzle are shown on the suction side of cascades. And the shocks formed at the leading edge of the 2nd blade looks diffused. This seemed to be caused by the 3D nozzle flow which is not uniform. Semicircle shapes observed at the 3rd blade is a mark of pinhole crack on window.

Fig. 18 ~ Fig. 24 show the visualized image of supersonic turbine for wide range of pressure ratio. Fig. 18 is the Shadowgraph image for pressure ratio of 4.2. The incidence angle of the rotor flow is positive. Detached shock is formed at the leading edge of the 2nd blade. Oblique shock is formed at the 10% axial chord downstream from the leading edge on the pressure side of the 1st blade. Flow is separated from the suction surface at the 45% axial chord downstream from the leading edge of the 2nd blade. Fig. 19 is the Shadowgraph image for pressure ratio of 5.25. The incidence angle of the rotor flow is positive. But the angle is smaller than Fig. 18. Weak normal shock is formed at the 35% axial chord downstream from the leading edge on the suction side of the 2nd blade. Flow is separated form the suction surface at the 45% axial chord downstream from the leading edge of the 2nd blade. Detached shock is formed at the leading edge of the 2nd blade. Fishtail shock is formed at the trailing edge of the 1st and 2nd blade. Fig. 20 is the Shadowgraph image for pressure ratio of 6.3. The incidence angle of the rotor flow is almost zero. Detached shock is formed at the leading edge of the 1st and 2nd blade. Angle of the detached shock on the suction side of the 2nd blade is smaller than Fig. 19. Flow is separated from the suction surface at the 40% axial chord downstream from the leading edge of the 2nd blade. Detached shock on the pressure side of the 1st blade meets the separated flow region on the suction surface of the 2nd blade. Fishtail shock is formed at the trailing edge of the 1st and 2nd blade. Fig. 21 is the Shadowgraph image for pressure ratio of 7.34. The incidence angle of the rotor flow is a little negative. Detached shock is formed at the leading edge of the 1st and 2nd blade. Angle of the detached shock on the suction side of the 2nd blade is smaller than Fig. 20. But the angle of the detached shock on the pressure side of the 1st blade is same with Fig. 20.

Flow is separated from the suction surface at the 40% axial chord downstream from the leading edge of the 2nd blade. The size of separated flow region is similar with Fig. 20. Detached shock on the pressure side of the 1st blade meets the separated flow region of the 2nd blade. Fishtail shock is formed at the trailing edge of the 1st and 2nd blade. Fig. 22 is the Shadowgraph image for pressure ratio of 8.39. The incidence angle of the rotor flow is more negative than Fig. 21. Detached shock is formed at the leading edge of the 1st and 2nd blade. Angle of the detached shock on the suction side of the 2nd blade is smaller than Fig. 21. But angle of the detached shock on the pressure side of the 1st blade is same with Fig. 21. Flow is separated from the suction surface at the 40% axial chord downstream from the leading edge of the 2nd blade. The size of separated flow region is similar with Fig. 21. Detached shock on the pressure side of the 1st blade meets the separated flow resion of the 2nd blade. Fishtail shock is formed at the trailing edge of the 1st and 2nd blade. Fig. 23 is the Shadowgraph image for pressure ratio of 10.48. The incidence angle of the rotor flow is more negative than Fig. 22. Detached shock is formed at the leading edge of the 1st and 2nd blade. Angle of the detached shock on the suction side of the 2nd blade is smaller than Fig. 22. But angle of the detached shock on the pressure side of the 1st blade is same with Fig. 22. Flow is separated from the suction surface at the 40% axial chord downstream from the leading edge of the 2nd blade. The size of separated flow region is similar with Fig. 22. Detached shock on the pressure side of the 1st blade meets the separated flow region of the 2nd blade. Fishtail shock is formed at the trailing edge of the 1st and 2nd blade. Fig. 24 is the Shadowgraph image for pressure ratio of 12.59. The incidence angle of the rotor flow is more negative than Fig. 21. Detached shock is formed at the leading edge of the 1st and 2nd blade. Angle of the detached shock on the suction side of the 2nd blade is smaller than Fig. 23. But angle of the detached shock on the pressure side of the 1st blade is same with Fig. 23. Flow is separated from the suction surface at the 40% axial chord downstream from the leading edge of the 2nd blade. The size of separated flow region is similar with Fig. 23. Detached shock on the pressure side of the 1st blade meets the separated flow region of the 2nd blade. Fishtail shock is formed at the trailing edge of the 1st and 2nd blade.

Detached shock formed at the leading edge of the 2nd blade pass into a blade passage as the pressure ratio increases. This is caused by the reason that the exit flow angle of nozzle (λ) increases while rotor flow incidence angle decreases as the pressure ratio increases. But, the angle of the detached shock on the pressure side of the 1st blade does not change regardless of the pressure ratio. And the size of separated flow region does not change a lot(Fig. 25).

Conclusions

In this study, the experiments have been performed to analyze the flow characteristic including the shock pattern of partial admission supersonic impulse turbine with a small wind tunnel. These experiments were focussed on visualization of nozzle and turbine cascade flows over a wide range of the pressure ratio. The followings are concluded by the experiments:

1. Shock pattern of the nozzle exit points(A, B point of Fig. 8) is changed by the pressure ratio.

2. As the pressure ratio increases, nozzle exit flow of the part A(Fig. 8) is bent more inward with oblique shock while the flow around part b (Fig. 8) is spreaded out more with expansion waves.

3. Nozzle exit flow angle is increased as the pressure ratio increases resulting in the decrease of rotor incidence angle.

4. Detached shock angle on the pressure side of the 1st blade does not change with the variation of the pressure ratio.

5. Detached shock angle on the suction side of the 2nd blade is decreased as the pressure ratio increase resulting in the decrease of rotor incidence angle.

6. The effect of pressure ratio on the size of the separated flow region is small.

References

1. Langston, L.S., Nice, M.L. and Hooper, R.M., 1977, "Three-Dimensional Flow Within a Turbine Cascade Passage", *Trans. of the ASME, J. of Eng. for Power,* Vol. 99, pp. 21-28.

2. Kiock, A., Lehthaus, F., Baines, N.C. and Sieverding, C.H., 1986, "The Transonic Flow through a Plane Turbine Cascade as Measured in Four European Wind Tunnels", *Trans. of the ASME, J. of Eng. for Gas Turbines and Power.* Vol. 108, pp. 277-85.

3. Ainley, D.G., and Mathieson, G.C.R., 1951, "A Method of Performance Estimation for Axial Flow Turbines", *British ARC*, R&M 2974.

4. Dunham, J., and Came, P.M., 1970, "Improvements to the Ainley/Mathieson Method of Turbine Performance Prediction", *ASME Journal of Engineering for Power*, pp. 252-256.

5. Colclough, C. D., 1966, "Design of turbine blades suitable for supersonic relative inlet velocities and the investigation of their performance in cascades: part II experiments, results and discussion", *Journal of Mechanical Engineering Science*, 8 (No. 2).

6. Stratford, B. S. and Sansome, G. E., 1965, "Theory and tunnel tests of rotor blades for supersonic turbines", *R&M 3275.*